Clinical Cancer Research

Deletion of 11q in Neuroblastomas Drives Sensitivity to PARP Inhibition

Elena Sanmartín[1,2], Lisandra Muñoz[1,2], Marta Piqueras[3], J. Antoni Sirerol[1,2], Pablo Berlanga[2,4], Adela Cañete[2,4], Victoria Castel[2,4], and Jaime Font de Mora[1,2]

Abstract

Purpose: Despite advances in multimodal therapy, neuroblastomas with hemizygous deletion in chromosome 11q (20%–30%) undergo consecutive recurrences with poor outcome. We hypothesized that patients with 11q-loss may share a druggable molecular target(s) that can be exploited for a precision medicine strategy to improve treatment outcome.

Experimental Design: SNP arrays were combined with next-generation sequencing (NGS) to precisely define the deleted region in 17 primary 11q-loss neuroblastomas and identify allelic variants in genes relevant for neuroblastoma etiology. We assessed PARP inhibitor olaparib in combination with other chemotherapy medications using both *in vitro* and *in vivo* models.

Results: We detected that *ATM* haploinsufficiency and *ATM* allelic variants are common genetic hallmarks of 11q-loss neuroblastomas. On the basis of the distinct DNA repair pathways triggered by ATM and PARP, we postulated that 11q-loss may define a subgroup of neuroblastomas with higher sensitivity to PARP inhibitors. Noteworthy, concomitant treatment with olaparib and DNA alkylating agent temozolomide potently inhibited growth of cell lines harboring 11q-loss. This drug synergism was less potent when temozolomide was exchanged for cisplatin or irinotecan. Intact 11q cells concomitantly treated with ATM inhibitor displayed growth arrest and enhanced apoptosis, revealing a role for ATM in the mechanism that mediates sensitivity to temozolomide–olaparib. Interestingly, functional TP53 is required for efficacy of this treatment. In an *in vivo* model, coadministration of temozolomide–olaparib resulted in sustained xenograft regression.

Conclusions: Our findings reveal a potent synergism between temozolomide and olaparib in treatment of neuroblastomas with 11q-loss and provide a rationale for further clinical investigation.
Clin Cancer Res; 23(22); 6875–87. ©2017 AACR.

Introduction

Neuroblastoma is the most common extracranial solid tumor in pediatric patients. High-risk patients continue to have very poor clinical outcomes despite intensive therapeutic interventions. Analysis of chromosomal alterations using FISH revealed that chromosomal alterations in 11q, 3p, 1p, and *MYCN* define four different groups, all with increased risk for disease progression (1). In this classification, 11q and *MYCN* alterations are particularly interesting because they are of higher incidence (about 30% and 20%, respectively, for all neuroblastoma cases) and constitute very valuable markers for predicting recurrence and prognosis. In contrast to the faster relapse of *MYCN*-amplified neuroblastomas, patients with 11q deletion display longer periods of recurrence but still face an inevitable fatal outcome. Therefore, finding effective therapeutic targets for this genetic alteration remains a priority in precision oncology.

The hypothesis that the 11q contains genes implicated in neuroblastoma development has formed the basis of studies aimed at identification of the alterations triggered by deletion of this chromosomal region. Profiling of neuroblastomas with and without 11q deletion identified a number of genes whose altered expression correlated highly with 11q-loss (2); however, none of these genes actually map to 11q. Thus, it remains to be determined how loss of genetic information in 11q modulates neuroblastoma development and/or outcome. Indeed, chromosomal deletion in 11q is highly correlated with relapse and metastasis (3), suggesting a causal relationship between this region and disease outcome. Other genomic profiling studies have suggested the existence of two subgroups of patients who bear the 11q chromosomal alteration, each with a distinct clinical phenotype and gene expression profile (4). This subdivision of 11q neuroblastomas is further supported by the differential expression of miRNAs within distinct subgroups of neuroblastomas (5). The expression of 11q hybrid proteins fused to FOXR1 transcription factor as a result of microdeletions and intrachromosomal fusion genes have also been reported (6).

11q deletion generally confers high risk and has been associated with alterations of tumor suppressors in this chromosomal region (7). *H2AFX* has been postulated to play a role in this type of neuroblastoma (8). Expression of *TSLC1*, a gene in the same

[1]Laboratory of Cellular and Molecular Biology, Instituto de Investigación Sanitaria La Fe, Valencia, Spain. [2]Clinical and Translational Research in Cancer, Instituto de Investigación Sanitaria La Fe, Valencia, Spain. [3]Department of Physiology, School of Medicine, University of Valencia, Valencia, Spain. [4]Pediatric Oncology Unit, Hospital Universitario y Politécnico La Fe, Valencia, Spain.

Note: Supplementary data for this article are available at Clinical Cancer Research Online (http://clincancerres.aacrjournals.org/).

Corresponding Author: Jaime Font de Mora, Fundación para la Investigación Hospital La Fe, Torre A, 5-07, Avda. Fernando Abril Martorell, no. 106, Valencia 46026, Spain. Phone: 349-6124-6646; Fax: 349-6124-6232; E-mail: jaime.fontdemora@gmail.com

doi: 10.1158/1078-0432.CCR-17-0593

Translational Relevance

We observed that *ATM* haploinsufficiency and *ATM* allele variants are frequent genetic hallmarks in neuroblastomas with 11q deletion. Cell lines harboring 11q-loss express low levels of ATM and treatment of these cells with the PARP inhibitor olaparib and DNA alkylating agent temozolomide caused significant growth inhibition and apoptosis. The combination of olaparib with irinotecan or cisplatin was less efficient than when administered with temozolomide. Noteworthy, sensitivity to this olaparib–temozolomide combination therapy was dependent on functional TP53 and loss of *ATM* within 11q deletion. As *TP53* mutations are rare in primary neuroblastomas but have higher incidence upon relapse, the olaparib–temozolomide combination would have greater chances of success as first-line therapy. In an *in vivo* model, coadministration of olaparib and temozolomide caused sustained tumor regression. Hence, our results reveal enhanced synergism between temozolomide and olaparib in 11q-loss neuroblastomas with functional TP53 and provide a rationale for precision medicine based on tumor genetics.

chromosomal locus, has been correlated with poor outcome and its ectopic expression in the cell line SH-SY5Y reduces proliferation, suggesting that *TSLC1* acts as a tumor suppressor in neuroblastomas (9). The ubiquitin ligase *UBE4A* has also been mapped to this chromosomal region (10). UBE4A plays a relevant role in chromosomal condensation and segregation by polyubiquitylation of securin, hence, targeting securin for proteasomal degradation (10). The pathologic implication of UBE4A in the disease might explain the rapid development of resistance to the proteasome inhibitor bortezomib. These observations underscore the urgent need for novel therapeutic strategies to treat neuroblastomas with 11q deletion.

We have previously shown that proteasome inhibition in combination with retinoic acid delays relapse by enhancing differentiation and death of neuroblastoma stem cells (11). This combination therapy may be appropriate for certain types of neuroblastomas but we have no evidence that it would also target genetic alterations occurring concomitantly with 11q deletion. In this regard, our previous studies demonstrate that *MYCN*-amplified metastatic neuroblastoma has a poor survival with conventional therapy, even with intensive treatment (12). However, in contrast to *MYCN*-amplified neuroblastomas, neuroblastomas with deletion in 11q display a high frequency of chromosomal breaks (8), revealing a phenotype of high chromosomal instability related to or localized within 11q. Thus, one plausible explanation for the association of 11q with poor clinical outcome is that this region contains genes implicated in DNA repair. Interestingly, the minimal deleted region shared by most of neuroblastomas is telomeric for *ATM* and *PP2R1B* genes (13). The ataxia telangiectasia gene (*ATM*), localized in 11q22-q23, plays an essential role in maintaining genomic integrity by regulating the repair of double-strand DNA breaks and activating the different checkpoints throughout the cell cycle. *ATM* has been associated with development of some subtypes of sporadic lymphoma and leukemia, but is poorly studied in neuroblastoma disease (14). Collectively, these observations suggest that *ATM* could have a direct role in the development of neuroblastomas with 11q deletion.

Materials and Methods

Patients and samples

This study included 412 patients diagnosed with neuroblastoma between years 2008 and 2016 in Spanish cooperative hospitals (SEHOP; 6 patients with concomitant *MYCN* amplification and 11q deletion were excluded of the statistical analysis). Staging and risk stratification were established according to International Neuroblastoma Staging System (INSS) and International Neuroblastoma Risk Group (INRG; ref. 15). Patient's median follow-up was 33 months (range 1–100 months). The distribution of patients by stages was 24% stage 1; 10% stage 2; 18% stage 3; 37% stage 4 and 11% stage 4S. Median age of the cohort at diagnosis was 15 months (first quartile 5 months, third quartile 44 months). Information about clinical parameters of this patient cohort is detailed in Supplementary Table S1. Neuroblastoma primary tumors of untreated patients were centrally reviewed and histologic type was classified according to the International Neuroblastoma Pathology Classification (INPC) criteria (16, 17).

Biological studies included status of *MYCN* (studied by FISH) and 11q (studied by MLPA from 2008–2012 and by CytoScan HD arrays from 2013–2016), according to ENQUA guidelines (18, 19). *MYCN* was amplified in 15% of patients (5 of them with heterogeneous amplification), 11q was deleted in 24% and not amplified and with no 11q deletion in 61% of patients. Patient's follow-up was obtained from Spanish neuroblastoma studies database. The study was conducted in accordance with the reporting recommendations for tumor marker prognostic studies (REMARK), the Declaration of Helsinki and La Fe Research Ethics Committee approved this project. Parents or legal guardians signed an informed consent statement for sample and data management.

DNA extraction and SNP array analyses

SNP dataset has been deposited in NCBI's Gene Expression Omnibus and are accessible through GEO Series accession number GSE101533 (https://www.ncbi.nlm.nih.gov/geo/query/acc.cgi?acc=GSE101533). Genomic DNA was extracted from frozen tumor tissues by a standard proteinase K and phenol–chloroform extraction protocol. Quantity and quality of DNA was assessed by NanoDrop spectrophotometer absorbance (Thermo Fisher Scientific), gel electrophoresis, and second quantification after PCR amplification. Patients' samples and cell lines used for sequencing were also analyzed by molecular karyotyping with SNP arrays (Cytoscan HD, Affymetrix). Fragmented DNA by Nsp I digestion was further ligated to adaptor followed by PCR amplification. The PCR product was hybridized using Affymetrix CytoScan HD Array Gene Chip and processed with the Fluidic Station (Affymetrix). SNP array results were analyzed with Chromosome Analysis Suite software (Affymetrix, ChAS; version 3.1). The annotation version used by the ChAS software is based on the February 2009 human reference sequence GRCh37 (hg19). SNP array data quality was assessed with the internal array quality control parameter "median of the absolute values of all pairwise differences" (MAPD). SNP array data were plotted and interpreted as described previously (20). Briefly, circos plots were created by extracting weighted $\log_2$ ratio and allele peaks information from Affymetrix software ChAS (ChAS 3.1). Individual weighted $\log_2$ ratio probes were binned

into groups of 100 and the bin average taken as smoothed signal. Allele peaks were trimmed to values between 0 and 1. Both smoothed weighted $\log_2$ ratio and allele peaks were plotted using the Circos software v0.68-1. Smoothed weighted $\log_2$ ratio values ≥ 0.15 are shown in blue (gain) and LRR values ≤ -0.15 in red (loss).

Next-generation sequencing

Sequencing analysis was performed on the Genomic Unit of La Fe Hospital Research Institute for 17 neuroblastoma cases and 7 cell lines. Sequence dataset GSE101989 was deposited at https://www.ncbi.nlm.nih.gov/geo/query/acc.cgi?acc=GSE101989 and is combined with SNP dataset in superSeries GSE101990 available at https://www.ncbi.nlm.nih.gov/geo/query/acc.cgi?acc=GSE101990. Quality and quantity of DNA was determined by Qubit dsDNA HS Assay Kit (Invitrogen). *ATM* gene (NM_000051.3) was sequenced with Human Comprehensive Cancer Panel (Qiagen), containing exons 2–63, with partial coverage in exons 2, 6, 25, 28, 49, and 63. Additional variants were also studied by this sequencing panel. Amplicon library was prepared using GeneRead DNAseq Targeted HC Panel V2 (NGHS-501X-12, Qiagen) according to manufacturer's instructions. DNA high-throughput sequencing was performed on Ion Proton instrument using Ion PI HiQ Sequencing Kit on the Ion PI sequencing chip (Thermo Fisher Scientific). Data from the Ion Torrent runs were analyzed using the platform-specific pipeline software Torrent Suite v5.0. The sequence variants in each sample were identified using the Torrent Suite Variant Caller (TSVC; v4.0-r76860) plug-in and browser extensible data (BED) files (chromosome coordinates) that specify the coding regions of the target genes within the human reference genome (hg19) retrieved from the NCBI database (build 37) as a reference. Finally, Ion Reporter software (https://ionreporter.thermofisher.com) was used to further annotate variant caller format (VCF) files and Integrated Genomic Viewer (IGV) software (21) was then used to complete the visualization and to discriminate false-positive variants. We considered only variants with balanced numbers of forward and reverse reads. Any variant found in *ATM* was confirmed by Sanger to avoid false positives.

MRE11A gene (NM_005591.3) was sequenced with ClearSeq Inherited Disease XT panel (Agilent Technologies) covering exons 2–20. Library preparation was done with ClearSeq XT Capture Libraries (Agilent Technologies). Finally DNA high-throughput sequencing was performed on NextSeq500 (Illumina Technologies) with a Mid-Output flow cell for paired 150-cycle reads. Each procedure was realized following the manufacturer's instructions. Reads were trimmed and filtered with PrinSeq and further mapped against the latest human reference genome GRCh38 with BWA MEM (22). Read duplicates were removed with PicardTools (http://broadinstitute.github.io/picard). Variants were called with the Haplotype caller software from the GATK package according to GATK Best Practices recommendations (23). Variant calls were then annotated using the variant effect predictor tool from the set of tools of the Ensembl 86 release.

Variant calls with minor allele frequency (MAF) of > 1% were excluded from further analyses. MAF numbers provided by Ion Reporter Software used the source 1000 Genomes Project (http://www.internationalgenome.org), containing data of 2,504 individuals from 26 populations and reporting the minor allele frequency for each rs (reference SNP ID number) in a default global population. Investigation about the potential pathogenic role was done using databases [COSMIC, dbSNP, ClinVar (NCBI)] and prediction algorithms (SIFT, PolyPhen-2, or Mutation Taster). *H2AFX* (NM_002105) full sequencing was done by Sanger with the pair of oligos 5′-GTCCTGGGGGCTTATAAAGG-3' and 5′-GCTCAGCTCTTTCCATGAGG-3'.

Cell culture and treatments

SK-N-BE(2) and SH-SY5Y cell lines were purchased from ATCC in 2010. IMR-32 cells were kindly provided by R. Versteeg and NLF, NBL-S, LA-N-1, and SK-N-AS were kindly provided by F. Spelemann, both in 2013. Cell lines were maintained in DMEM with L-glutamine and L-glucose (HyClone) supplemented with 10% v/v FBS, 50 U/mL penicillin, and 50 mg/mL streptomycin and incubated in a humidified 5% CO_2 air atmosphere at 37°C. No more than 40 passages were done after thawing. Cell lines were checked for mycoplasma every 6 months with VenorGeM detection kit (Minerva Biolabs; last check up in February 2017) and were authenticated by NGS and SNP arrays (Supplementary Table S3; Supplementary Fig. S3).

Cells were treated with DNA alkylating agent temozolomide (100 μmol/L) and/or with the PARP inhibitor olaparib (AZD2281; 10 μmol/L). Untreated control cells were cultured in the presence of vehicle alone (0.1% DMSO). For the inhibition of ATM kinase activity, cells were treated with KU-60019 (10 μmol/L). Temozolomide was purchased from SIGMA, KU-60019, and irinotecan (SN-38) were purchased from Selleckchem, cisplatin from Pharmacia Nostrum, and olaparib was a gift from AstraZeneca.

To establish the working concentration of chemotherapy drugs causing about 60%–80% cell viability alone, we initially treated for 3 days the neuroblastoma cell line IMR-32 with increasing doses (temozolomide ranging from 30 to 1,000 μmol/L; cisplatin from 0.3 to 10 μmol/L; irinotecan (SN-38) from 0.5 to 100 nmol/L). In addition, we also tested olaparib at decreasing concentrations (10, 3, and 1 μmol/L). For proliferation/survival assays, cells were seeded at a density of $3–10 \times 10^3$ cells per well in 96 well-plates and subsequently analyzed by XTT colorimetric assay (Cell Proliferation Kit II XTT, Roche) measuring absorbance at 450 nm. All assays were performed in triplicate in at least two independent experiments, and data were expressed as the mean ± SE. Thus, we administrated temozolomide 100 μmol/L, cisplatin 0.3 μmol/L, and irinotecan (SN-38) 0.5 nmol/L.

To analyze the synergistically inhibitory effect between cytotoxic agents and olaparib, the coefficient of drug interaction (CDI; ref. 24) was calculated as follows: CDI=AB/(A × B). According to the absorbance of each group, AB is the ratio of the two-drug combination group to the control group and A or B is the ratio of the single drug group to the control group. Therefore, CDI < 1 indicates synergism, CDI < 0.7 indicates a significantly synergistic effect, CDI = 1 indicates additivity, and CDI > 1 indicates antagonism.

Live/dead cell detection assay by flow cytometry

To analyze live and dead cells using flow cytometry, we used LIVE/DEAD Fixable Near-IR Dead Cell Stain Kit (Invitrogen) according to the manufacturer's recommendations. Briefly, subconfluent cells were treated with temozolomide and olaparib as described above for 1 day and 3 days, respectively. Supernatant and cells were collected, washed, and resuspended in PBS at density 10^6 cells/mL. Near-IR fluorescent reactive dye L10119 was added at 1 μL/mL, incubated for 30 minutes without light at

room temperature. Cells were pelleted, washed, and further resuspended in 0.9 volumes of PBS with 0.1 volumes of 37% formaldehyde (Sigma) for 15 minutes at room temperature. Cells were washed and resuspended in 1 volume of PBS + 1% BSA before flow cytometry analysis. We used a FACSCanto-II flow cytometer (Becton Dickinson) and at least 20,000 events were acquired with FACSDiva software at 775 nm and analyzed with Infinicyt software (Cytognos).

Transfection of wild-type *TP53* and caspase-3/7 assay

SK-N-AS cells were seeded in 6-well plates and grown to about 80% confluency at transfection. Each well was transfected with 2.5 μg of the plasmid pCB6+p53 containing human *TP53* wild-type cDNA using Lipofectamine 2000 kit (Invitrogen), according to the manufacturer's protocol. Cells were incubated 2 days following transfection prior to further treatment with temozolomide (100 μmol/L) and/or olaparib (10 μmol/L). Cells were harvested 24 hours posttreatment and lysed for Western blot analysis. Enzymatic activity of caspase-3/7 was determined with caspase-3/7 Glo kit (Promega) in 96-well plates 2 days after transfection and 1 day after drug treatment. Luminescence was measured in a Biotek Synergy H1 microplate reader and normalized against total protein determined by colorimetric Bradford assay.

Pharmacologic inhibition of TP53 and *TP53* knock down

NBL-S and IMR-32 cells were seeded in 6-well plates and grown to about 80% confluency. Cells were transfected with 25 pmol/L annealed siTP53 (catalog no. 16104, Ambion) using Lipofectamine RNAiMAX (Invitrogen), according to the manufacturer's protocol. TP53 inhibition was induced with Pifithrin-α (PFT-α, 10 μmol/L; P4359, Sigma). Cells were incubated for 1 day after siTP53 transfection or inhibition and were further treated with temozolomide (100 μmol/L) plus olaparib (10 μmol/L in NBL-S and 1 μmol/L in IMR-32) or vehicle alone (DMSO). Cells were harvested 24 hours posttreatment and lysed for Western blot analysis.

Antibodies

mAbs were used as follows: caspase-3 (clone 8G10) and cleaved caspase-3 (Asp175, 5A1E) from Cell Signaling Technology; anti-p53 (clone DO-1, Santa Cruz Biotechnology); anti-β-actin (clone AC-15, Sigma-Aldrich), and anti-ATM (clone 2C1, Thermo Fisher Scientific). In addition, we used polyclonal antibody anti-PARP (Cell Signaling Technology). As secondary antibodies, we used anti-rabbit IgG peroxidase and anti-mouse IgG peroxidase (Sigma-Aldrich).

Western blotting

Cells were grown to about 80% confluence in 100-mm dishes and treated for 48 hours as indicated in each experiment. Conventional lysates were done with the following buffer: Tris-HCl 20 mmol/L, pH 7.5, NaCl 300 mmol/L, NaF 1 mmol/L, Na_2EDTA 1 mmol/L, EGTA 1 mmol/L, β-glicerolphosphate 1 mmol/L, Na_3VO_4 1 mmol/L, Triton X-100 1%, supplemented with protease cocktail inhibitors (Roche) and AEBSF 1 mmol/L (Roche). Proteins were transferred to Hybond-P membrane (Amersham Life Sciences), and blotted with the indicated antibodies. The membrane was probed for anti-β-actin as loading control. Proteins were visualized using enhanced chemiluminescence detection reagents (Pierce).

Xenografts

Experiments were conducted according to the European Community and Spanish regulations for the use of experimental animals and approved by the Institutional Committee of Animal Research. We used 8-week-old 12 BALB/c (CAnN.Cg-Foxn1nu/Crl) nu/nu mice per branch (6 males and 6 females). Each mouse was subcutaneously injected into the flanks with 1.5×10^7 IMR-32 cells resuspended in 0.2 mL PBS:Matrigel (1:1). Two weeks later, mice were orally treated for five consecutive days with olaparib (10 mg/kg) and/or temozolomide (50 mg/kg) resuspended in DMSO at 20 mg/mL and 100 mg/mL, respectively (10 μL/mouse/day per 20 g body weight). Control mice were treated with vehicle alone. Xenografts growth were measure every two or three days with a caliper and tumor volume was calculated by use of the modified ellipsoid formula $1/2(\text{length} \times \text{width}^2$; ref. 25).

Statistical analysis

Statistical analyses were performed using IBM SPSS Statistics version 21 (SPSS Inc.). The survival curves were plotted according to the Kaplan–Meier method and comparisons were done by log-rank test. Relapse-free survival (RFS) was defined as the time from diagnosis to the time of first occurrence of relapse, progression, or last follow-up, and overall survival (OS) was defined as the time from diagnosis until death or until last follow-up if the patient was alive. $P < 0.05$ was considered statistically significant.

Results

Hemizygous deletion in chromosome 11q undergo consecutive recurrences with poor outcome

Allelic deletion in 11q is a frequent chromosomal alteration occurring in high-risk neuroblastomas that inversely correlates with *MYCN* amplification (13, 26, 27). We studied outcome in a Spanish cohort of 412 neuroblastoma patients (Supplementary Table S1) and found that those with 11q deletion underwent frequent relapses comparable to those with *MYCN* amplification (Fig. 1A). Overall survival was also significantly low, although not as severe as in those with *MYCN* amplification (Fig. 1B). As expected, both *MYCN*-amplified and 11q-loss significantly associated with patient age (older than 18 months), stage 4, relapse/progression, and death (Supplementary Table S2). In contrast to *MYCN*-amplified neuroblastomas, 11q-deleted neuroblastomas display a high frequency of chromosomal breaks (8), revealing a phenotype with high chromosomal instability related or localized within 11q. One plausible explanation is that 11q contains genes implicated in DNA repair.

Haploinsufficiency and allelic variants in *ATM* are genetic hallmarks in 11q-deleted neuroblastomas

To characterize and precisely define the deleted region in 11q, we analyzed 17 11q-deleted neuroblastomas by molecular karyotyping and by next-generation sequencing (NGS), with the aim of identifying mutated genes relevant for neuroblastoma etiology and prognosis. The deleted region in these tumors was variable in length, frequently reaching the 11q subtelomeric region (Table 1). All neuroblastomas had multiple segmental breaks distributed through the whole karyotype (Supplementary Fig. S1), further supporting the hypothesis that 11q deletion may alter DNA repair. Interestingly, only two neuroblastomas had chromothripsis (10 or more consecutive segmental breaks within the same chromosome), TI_423 in chromosome 5 (Supplementary Fig.

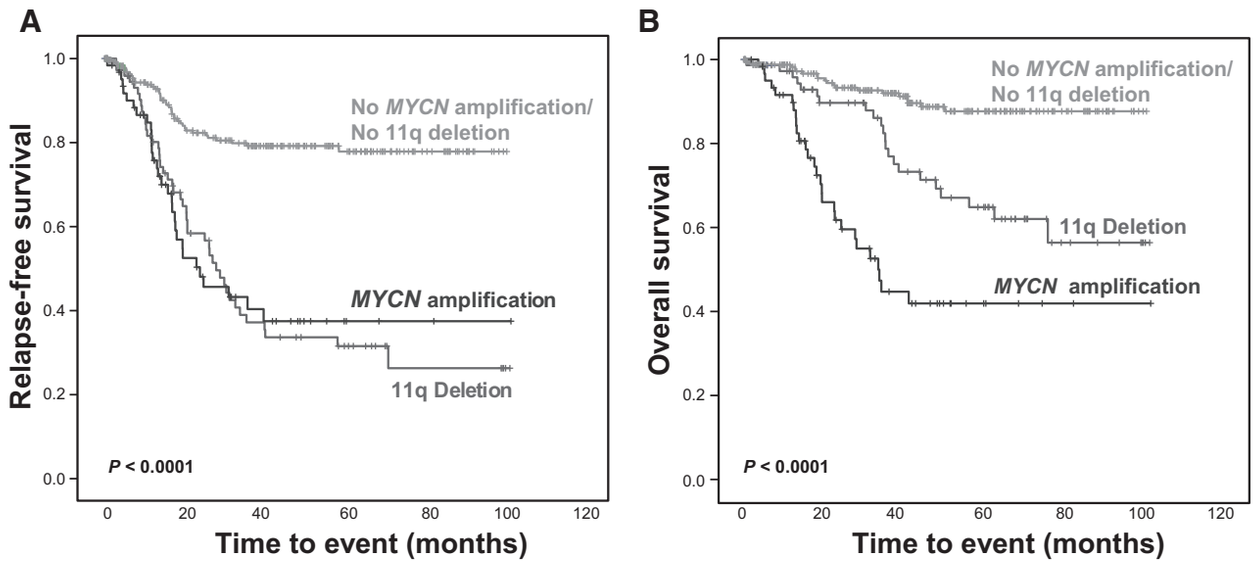

Figure 1.

Kaplan–Meier curves for 412 neuroblastoma patients according to *MYCN* amplification or 11q deletion (Spanish Neuroblastoma Registry). Relapse-free survival (**A**) and overall survival (**B**). Censored cases are denoted as crosses along the plots. Log-rank *P* values were used to compare survival curves between the three subgroups of neuroblastoma patients. Six cases with both *MYCN* amplification and 11q deletion were omitted from the statistical analysis.

S2A), and NBX_19 in chromosome 17 (Supplementary Fig. S2B). The smallest 11q-deleted region of overlap was 104934658 – 119216493 (hg19 coordinates). Three genes involved in DNA repair by homologous recombination were always included within the overlap deleted region: the Ataxia Telangiectasia Mutated (*ATM*) gene and its downstream signaling targets *H2AFX* and *MRE11A*, with the exception of patient NBX_49 in which *MRE11A* was not included in the deleted region. Although the coverage was not complete for all exons, our results reveal *ATM* rare allele variants in 8 of 17 cases, whereas no variants were found in *MRE11A* or *H2AF*X. Predictors for disease-causing variants support a pathogenic character or unknown significance for these variants (Supplementary Table S3).

Inhibition of cell growth and survival by olaparib and temozolomide in 11q-deleted cell lines

To assess the impact of *ATM* loss in 11q-deleted neuroblastomas, we chose the PARP inhibitor olaparib (AZD2281) as it has one of the lowest IC_{50} and inhibits PARP1, PARP2, and PARP3. In addition, olaparib has been studied in ATM-deficient lymphomas with promising results (28, 29). We used XTT colorimetric assay to test the proliferation and survival of several cell lines (Fig. 2A) cultured in the presence of olaparib (10 μmol/L) and temozolomide (100 μmol/L). We also tested olaparib at lower concentrations (1 and 3 μmol/L) which predictably were less efficacious (data not shown). Cell lines with intact 11q SK-N-BE(2) and SH-SY5Y (see Supplementary Fig. S3 for Molecular Karyotypes and Supplementary Table S3 for sequencing results) were resistant to the treatment (Fig. 2A). NLF cells, although resistant, showed a slower growth with the double treatment.

To evaluate whether resistance to combined treatment was related to intact 11q, we characterized the genetics of all cells lines used in the study. SK-N-BE(2) and NLF, but not SH-SY5Y, displayed 1p deletion/LOH as well as *MYCN* amplification (Supplementary Fig. S3). In contrast, the SH-SY5Y line contained the *ALK*-activating variant F1174L (Supplementary Table S3), as previously reported (30). We also detected the *ALK*-activating variant F1174L in LA-N-1 and *ALK* amplification in the NLF line (Supplementary Fig. S3). Interestingly, NLF also showed around 30% mosaic loss in chromosome 11, perhaps reflecting its mild sensitivity to the double treatment (Fig. 2A). Loss-of-function *TP53* variants found have been described previously for NLF, LA-N-1, and SK-N-BE(2) lines (31, 32).

In agreement with previous reports, our IMR-32 cells have 1p deletion and *MYCN* amplification (33) as well as *MEIS1* amplification (34). Notably, IMR-32 also displayed 17q gain and *ALK* amplification (Supplementary Fig. S3). We also detected 11q deletion as reported for IMR-32 parental cell line IMR-5 (13), but no *ATM* variants were identified (Supplementary Fig. S3 and Supplementary Table S3) in this line. These results contrast a recent publication which reported that this line has intact 11q but displays a pathogenic mutation in *ATM* (14). Consistent with our hypothesis, these cells harboring 11q deletion were highly sensitive to the concomitant treatment of olaparib plus temozolomide (Fig. 2A), perhaps due to *ATM* haploinsufficiency. 11q deletion was also detected in the NBL-S line (Supplementary Fig. S3), which was also sensitive to the combined therapy. LA-N-1 cells showed heterozygous allele variants in *ATM*, *CHEK2*, and *BRCA2*. This line contained intact 11q (Supplementary Fig. S3) but did not express ATM protein (Fig. 2B) and thus, displayed an intermediate sensitivity to the treatment.

In addition to growth and survival curves, we also determined the effect of combination treatment on the induction of cell death by flow cytometry analysis. The combination treatment significantly increased the percentage of dead cells in cell lines that were sensitive in growth and survival assays (IMR-32, NBL-S, and

Table 1. Genetic features in 11q-deleted neuroblastoma patients

Subject ID	Genomic coordinates for LOH in Chr11 (hg19):	Gene/s within or flanking segmental break	*ATM* variant[a]	*H2AFX* variant[b]	*MRE11A* variant[c]	Additional variants detected	Age at diagnosis (months)	*MYCN* amplification	Stage (INSS)	Stage (INRG)	Relapse/ Progression	RFS (months)	*Exitus*	OS (months)
NBX_17	69475848–135006516	CCND1, ORAOV1	No	No	No	*ALK* c.3939–8A>G	61	No	4	M	Yes	25	No	30
NBX_18	70765145–135006516	SHANK2	No	No	No	*NF1* T2581S; *TIAM1* I1249T	44	No	4	M	Yes	26	No	71
NBX_19	71658200–135006516	RNF121	No	No	ND		157	No	3	L2	Yes	15	Yes	96
NBX_29	75306138–135006516	ZBTB16	No	No	ND	*PIK3CA* M1043T	15	No	4	M	Yes	9	Yes	12
NBX_34	70014382–135006516	ANO1	D467H	No	No		23	Yes	2	L2	No	7	No	7
NBX_49	104934658–129698590	CARD17, NFRKB	F858L	No	No	*RET* Y791F	9	No	4S	MS	Yes	30	No	35
NBX_56	70847680–135006516	SHANK2	P604S	No	ND		55	No	4	M	Yes	70	No	75
NBX_6	71652484–135006516	RNF121, NUMA1	D1853V	No	No		4	No	4S	MS	Yes	9	No	31
TI_122	1–119216493	HMBS, H2AFX	No	No	No	*STK11* T367M	9	No	2A	L1	Yes	51	Yes	78
TI_423	83469247–135006516	DLG2, RAB30	No	No	ND		40	No	4	M	Yes	21	Yes	38
TI_494	82960723–135006516	RAB30, DLG2	F582L	No	ND		31	No	3	L2	Yes	10	Yes	13
TI_501	73228443–130270855	PHOX2A	V182L	No	No		39	Het	4	M	Yes	10	Yes	16
TI_672	74161738–135006516	KCNE3	No	No	ND	*ALK* R1275L	87	No	4	M	Yes	30	Yes	55
TI_719	72640418–135006516	PDE2A	No	No	No		60	No	4	M	Yes	58	No	59
TI_773	72176575–134924002	PDE2A	c.2805G>C	No	ND		43	No	4	M	Yes	19	Yes	35
TI_809	70299935–135006516	CTTN, SHANK2	No	No	No	*ALK* M1089T; *NF1* P654S	7	No	4S	MS	Yes	7	Yes	32
A786	70071006–135006516	FGF3, ANO1	W2344*	No	ND		9	No	3	L2	Yes	151	No	156

Abbreviations: Het, heterogeneous; ND, not determined.

[a]*ATM* (NM_000051.3) was sequenced with Human Comprehensive Cancer Panel (Qiagen), containing exons 2–63, with partial coverage in exons 2, 6, 25, 28, 49, and 63. Allelic variants were further validated by Sanger sequencing.

[b]Full sequencing of *H2AFX* (NM_002105) was done by Sanger.

[c]*MRE11A* (NM_005591.3) was sequenced with ClearSeq Inherited Disease Panel (Agilent Technologies) covering exons 2–20.

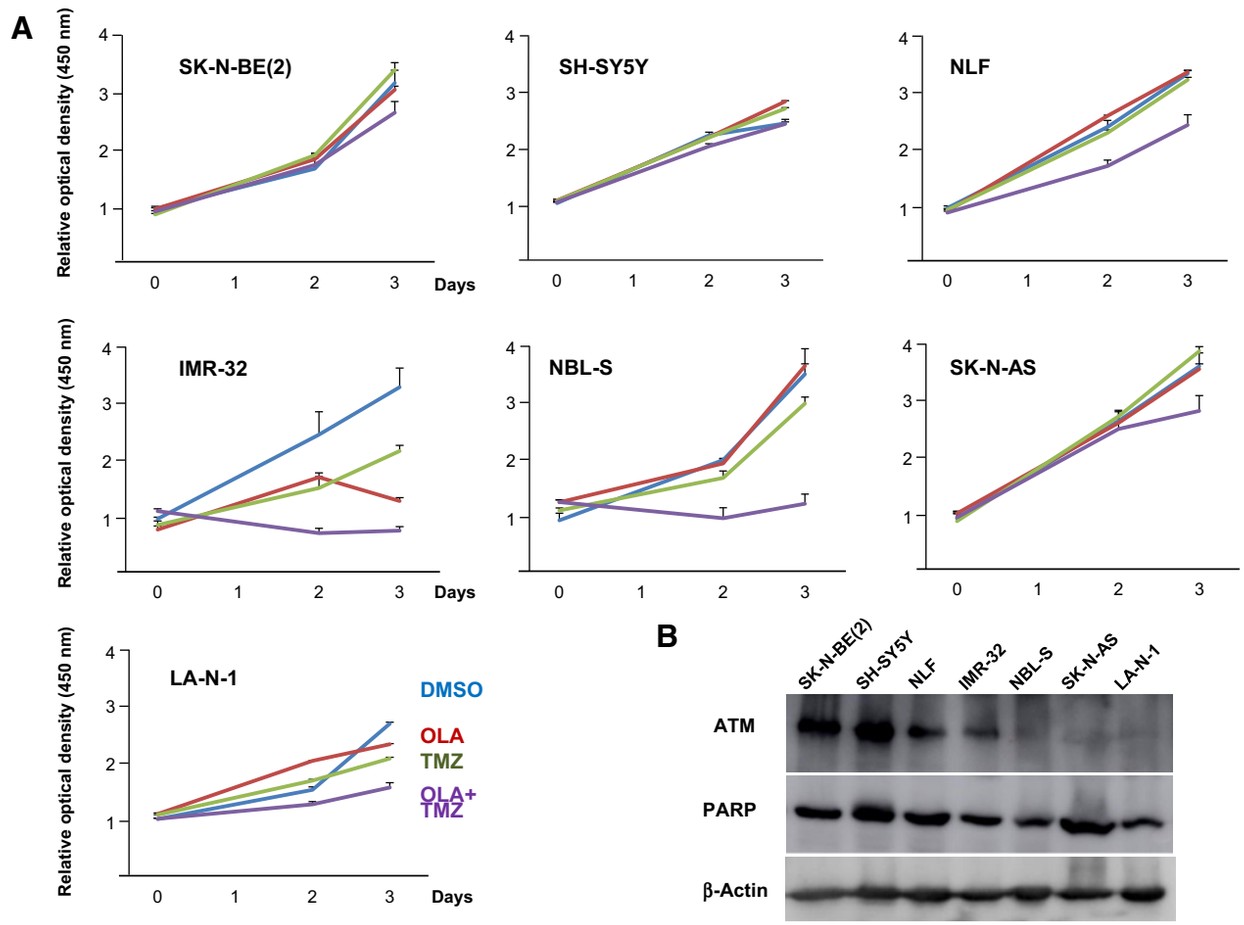

Figure 2.

Response of neuroblastoma cell lines to combined treatment with olaparib and temozolomide. **A,** Effects of drug treatment on cell growth curves. Neuroblastoma cell lines were grown in the presence of olaparib (10 μmol/L), temozolomide (100 μmol/L), both together, or vehicle alone (DMSO). Cell lines with 11q deletion: IMR-32, NBL-S, and SK-N-AS. Cell lines that do not have 11q deletion: SK-N-BE(2), SH-SY5Y, NLF, LA-N-1. **B,** Representative Western blot of ATM and PARP proteins in neuroblastoma cell lines. β-Actin was analyzed as a loading control.

LA-N-1; Supplementary Fig. S4). Similarly, cell lines that were resistant to combined treatment with temozolomide plus olaparib [SK-N-BE(2), SH-SY5Y, NLF, and SK-N-AS] did not display an increase in the percentage of dead cells (Supplementary Fig. S4). These results further support the notion that antitumoral effects of olaparib and temozolomide treatment are mediated, at least in part, by the induction of cell death.

Sensitivity to olaparib and temozolomide is mediated by TP53 and ATM

SK-N-AS cells were resistant to the treatment although they bear 11q deletion (Supplementary Fig. S3). Interestingly, these cells express inactive TP53 which is truncated in the C-terminus (31). Our NGS analysis of SK-N-AS line did not detect *TP53* exons 10 and 11, suggesting their ablation in these cells. We subsequently confirmed absence of exons 10 and 11 by PCR (Supplementary Fig. S5), consistent with previous reports (31, 32). Ectopic expression of wild-type *TP53* in SK-N-AS cells restored susceptibility to the combination treatment by increasing the levels of cleaved caspase-3 (Fig. 3A), increasing caspase enzymatic activity (Fig. 3B), and significantly reducing overall cell growth and survival (Fig. 3C). We then performed the converse approach in IMR-32 and NBL-S cells of knocking down TP53 expression with annealed oligos or inhibiting TP53 activity with the specific TP53 inhibitor pifithrin-α. Either strategy blunted the effects of combined treatment on caspase-3 cleavage in both cell lines, although siTP53 was more efficient (Fig. 3D and E). These studies further support a role for TP53 in the activation of apoptosis in response to temozolomide plus olaparib treatment. Interestingly, the combination treatment upregulated TP53 levels in NBL-S and SK-N-AS and to a lesser extent in IMR-32 cells, suggesting that TP53 forms part of the DNA damage response triggered by these agents. Collectively, these findings demonstrate that cell lines with 11q deletion are sensitive to olaparib plus temozolomide therapy and this response requires expression of functional TP53.

To further assess the role of ATM in neuroblastomas, we used SH-SY5Y cells that contain intact chromosome 11q and treated them with the specific ATM kinase inhibitor KU-60019. Treatment with the ATM inhibitor alone reduced cell growth and viability (Fig. 3F) but inhibition of ATM synergized with olaparib plus

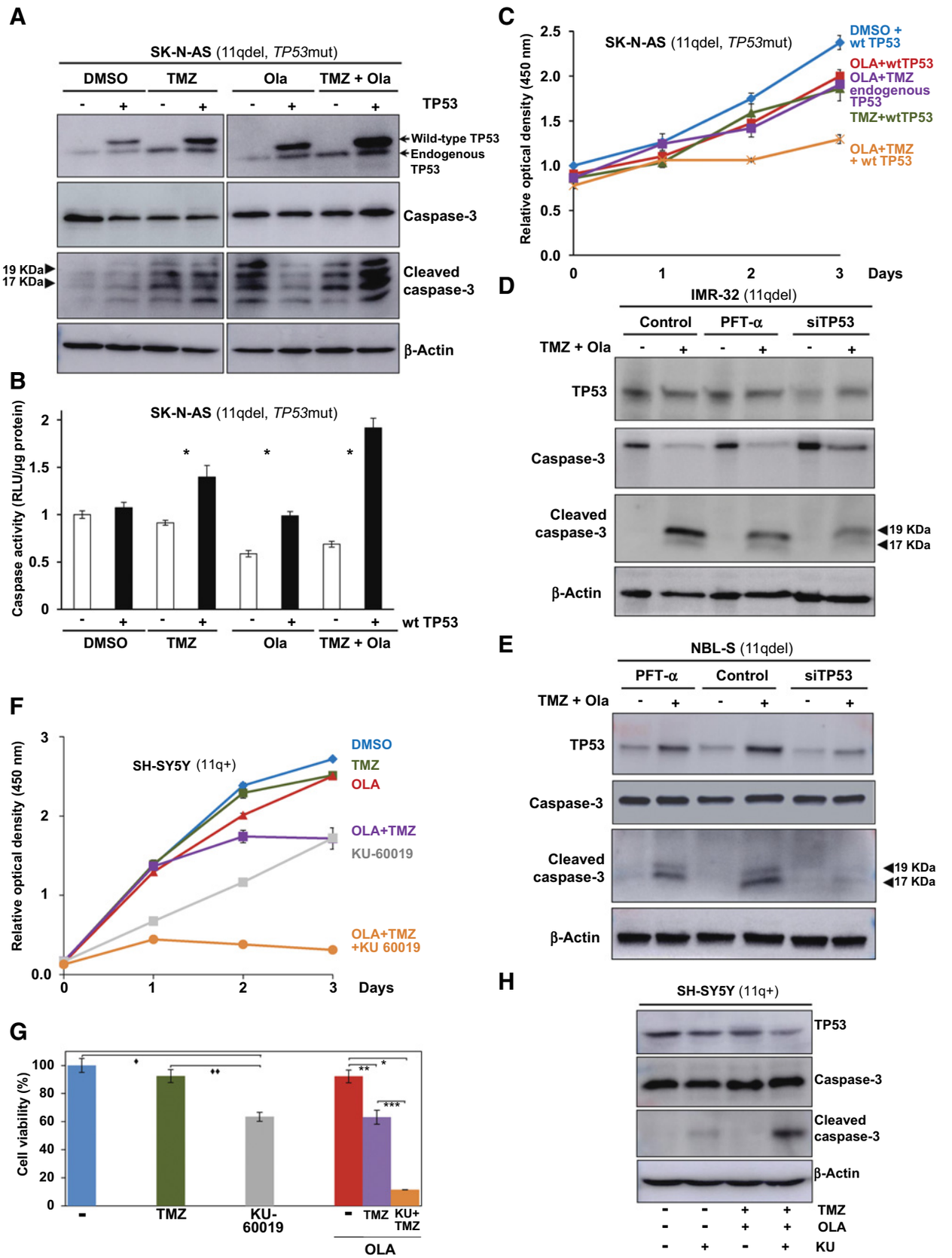

temozolomide [coefficient of drug interaction (CDI) = 0.26; Fig. 3G], suggesting that ATM expression and/or function determines sensitivity of tumor cells to this drug combination. The combined treatment of the ATM inhibitor with the two drugs potentiated the level of cellular apoptosis achieved by the inhibitor alone (Fig. 3H). These results strongly support the notion that loss of ATM expression and/or function is one mechanism required for cellular response to combination olaparib + temozolomide therapy.

Synergistic effect of olaparib with temozolomide

We used IMR-32 cells that harbor 11q deletion and functional TP53 to compare the efficiency of other chemotherapy drugs in combination with olaparib. We first determined the concentrations of temozolomide, cisplatin, or irinotecan which maintain cell viability at 60%–80% (Fig. 4A) and combined the drugs at these concentrations with olaparib (Fig. 4B). Treatment with olaparib and temozolomide displayed a synergistic effect (CDI = 0.26) and was more efficient at inhibiting cell growth and survival than when combined with cisplatin (CDI = 0.76) or with irinotecan (CDI = 0.67; Fig. 4C). Combination olaparib–temozolomide therapy was reported to be more efficacious in preclinical studies with Ewing sarcoma (35), although irinotecan required a lower dose than temozolomide. The combination with temozolomide induced apoptosis in IMR-32 cells (Fig. 4D). The synergistic effects of olaparib and temozolomide (CDI = 0.55) in NBL-S cells was also greater than olaparib and cisplatin (CDI = 0.70) or olaparib and irinotecan (CDI = 0.81). Notably, cell growth and survival were significantly restored by the caspase inhibitor Z-VAD-FMK (Fig. 4E), suggesting that the mechanism of action of temozolomide and olaparib occurs, at least in part, through the activation of caspase-3. Thus, we chose the combination temozolomide plus olaparib for a preclinical evaluation.

Efficient xenograft regression with combined olaparib and temozolomide

IMR-32 cells were transplanted in nude mice and used to assess combination therapy efficacy in xenograft model. Oral treatment for five consecutive days (one cycle) with olaparib and temozolomide resulted in a complete response/very good partial response of the tumor in all mice. These benefits were in sharp contrast to olaparib alone that only weakly inhibited xenograft growth or temozolomide alone where relapse of xenograft growth was noted after two weeks of treatment (Fig. 5A). Only 1 of 12 mice that received the combined chemotherapy showed a regrowth of the tumor during the fifth week after treatment, indicating that additional cycles of treatment may improve outcome.

Discussion

Hemizygous deletion of 11q is a frequent genetic marker in high-risk neuroblastomas but how this chromosomal aberration alters disease development and outcome remains poorly defined. Our retrospective analysis of neuroblastoma patients in Spain from 2008–2016 confirms the poorer outcome of patients with 11q-loss neuroblastomas (Fig. 1). These observations emphasize the urgent need for druggable targets in this subpopulation of patients. We carefully analyzed 17 primary neuroblastomas by SNP arrays and NGS for a panel of genes implicated in cancer initiation and progression. Although the coverage was not complete for all exons, our results reveal that *ATM* which encodes a crucial DNA repair protein was always contained within the deleted region and had an allele rare variant in 8 of 17 cases. These data suggest that haploinsufficiency for *ATM*, alone or in combination with other genetic variants, may have a relevant role in 11q-deleted neuroblastomas. *H2AFX* has also been implicated in this type of neuroblastoma (8) but we found no allelic variants in *H2AFX* or in *MRE11A*, suggesting that dysregulation of this pathway may be predominantly affected by combined haploinsufficiency or by *ATM* variants. The identified *ATM* variant P604S (Table 1) was recently reported in 3 of 50 neuroblastoma cases, 2 of them germline variants (14). This same variant was previously reported in Hodgkin lymphoma and associated with more aggressive clinical course of the disease (36).

Variant F582L has also been implicated in acute lymphoblastic leukemia (ALL; 37) and in risk of chronic lymphocytic leukemia (CLL; 38). This as well as other *ATM* variants may display variable pathogenic penetrance depending on other alterations occurring in the tumor. In this regard, it is possible that concomitant *TIAM1* variants may improve clinical outcome in neuroblastomas (39). F858L has been described in risk of CLL (38) and D1853V was reported pathogenic in B-cell chronic lymphocytic leukemia (40). We also detected a novel nonsense variant W2344*, which occurs in the FAT domain proximal to the phosphatidylinositol 3 and 4 kinase domain. One possibility is that these variants moderately alter ATM activity and their pathologic role depends on other concomitant alterations, including epigenetic changes that might explain the impact of *H2AFX*, *MRE11A*, or other 11q genes on the

Figure 3.

Sensitivity to olaparib and temozolomide depends on wild-type TP53 and loss of ATM function. **A,** Western blot analysis of TP53 and caspase-3 activation in SK-N-AS cell line. **B,** Enzymatic activity of caspase-3/7 was measured after 1 day of treatment under the same conditions as in **A** using Caspase-Glo-3/7 assay kit and values were normalized to protein levels. * indicates a significant difference ($P < 0.005$). **C,** Cell growth and survival curves of SK-N-AS cells transfected with wild-type TP53. One day later (day 0), cells were treated as indicated. Untransfected cells (endogenous TP53) were also treated with temozolomide and olaparib. Linear regression model with splines was performed to assess significance of the evolution between treatments with time: temozolomide (TMZ) + olaparib (OLA) + wt TP53 versus temozolomide + olaparib + endogenous TP53 ($P < 0.001$); DMSO + wt TP53 versus OLA + wt TP53 ($P = 0.008$); DMSO + wt TP53 versus TMZ + wt TP53 ($P = 0.015$); DMSO + wt TP53 versus TMZ+OLA + wt TP53 ($P < 0.001$). **D,** IMR-32 cells were transfected with siTP53 annealed oligonucleotides or treated with TP53-specific inhibitor 10 μmol/L pifithrin-α (PFT-α). On subsequent day, cells were treated with olaparib and temozolomide or with vehicle alone, as indicated. Cells were lysed and immunoblotted for the presence of cleaved caspase-3 as an indicator of apoptosis. **E,** NBL-S cells were treated as in **D** and cell lysates were analyzed by Western blot for the presence of cleaved caspase-3. **F,** ATM kinase activity was inhibited by addition of KU-60019 (10 μmol/L) in SH-SY5Y (11q+). This inhibitor promotes sensitive to olaparib and temozolomide treatment by reducing growth ratio and cell viability (**G**) after 72 hours of treatment. Linear regression model with splines was performed to assess significance of the evolution between treatments with time in **F**: $P < 0.001$ for DMSO versus KU60019, DMSO versus. Olaparib + temozolomide + KU60019 and KU60019 versus olaparib + temozolomide + KU60019. Statistical significance in **G** was determined by *t* test ♦, $P < 0.001$; ♦♦, $P < 0.001$; *, $P = 0.002$; **, $P = 0.01$; ***, $P = 0.001$. **H,** Western blot analysis of SH-SY5Y cells treated with temozolomide and olaparib. These drugs increased apoptosis when combined with ATM inhibitor KU-60019.

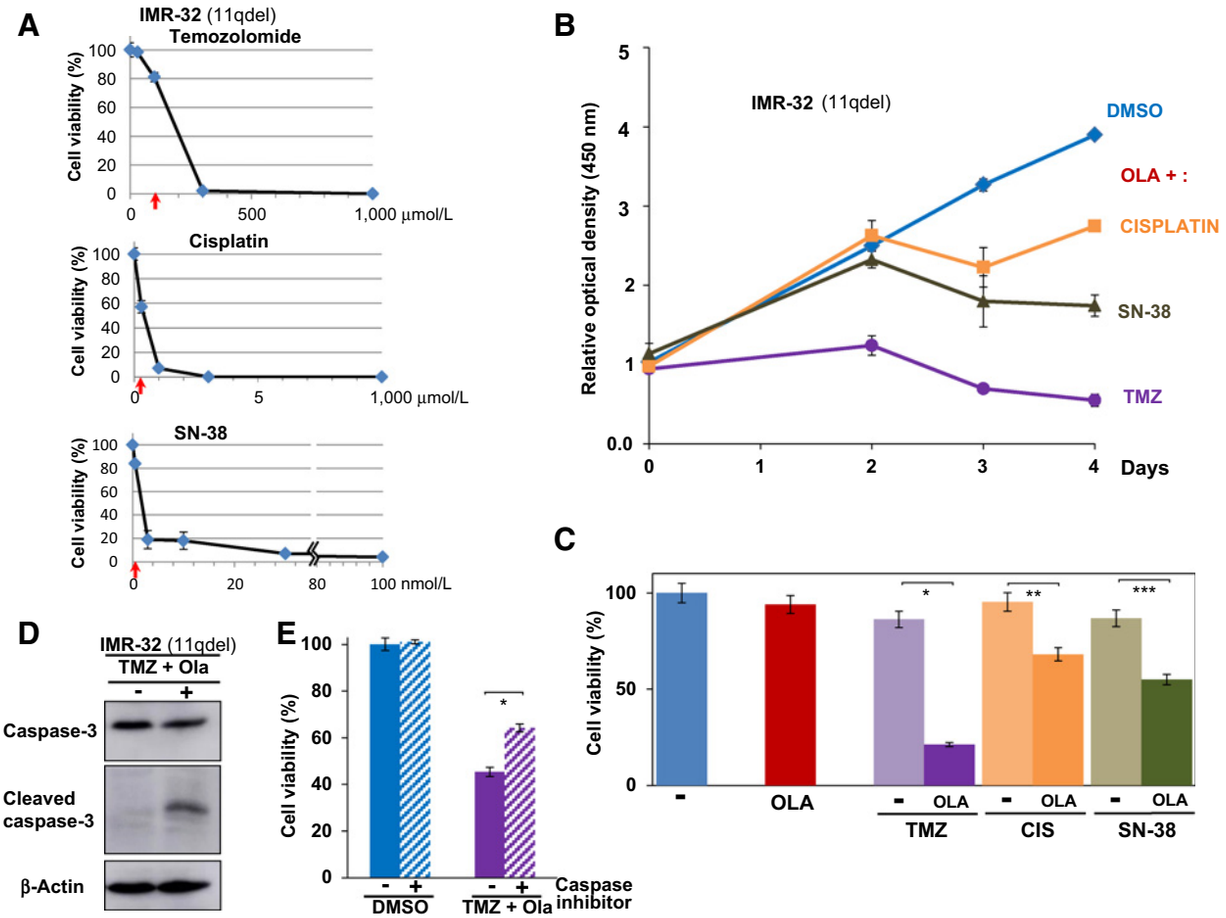

Figure 4.

Synergistic effect of temozolomide and olaparib in growth and survival inhibition. **A,** Dose-dependent toxicity of temozolomide (TMZ), cisplatin, and irinotecan (SN-38; 72 hours) in IMR-32 cells. **B,** Proliferation assay with IMR-32 cell, a cell line that harbors 11q deletion (11qdel), showed that olaparib (1 µmol/L) treatment in combination with temozolomide (100 µmol/L) inhibits more efficiently cell growth and survival than with either cisplatin (0.3 µmol/L) or with irinotecan (SN-38; 0.5 nmol/L). Linear regression models were performed to assess the interaction between day and treatment variables: $P = 0.003$ for DMSO versus olaparib (OLA) + cisplatin; $P < 0.001$ for DMSO versus olaparib + SN38; $P < 0.001$ for DMSO versus olaparib + temozolomide. **C,** Cell viability rate after 72 hours of treatment revealed synergistic effect between temozolomide and olaparib combination. Statistics significance was determined by *t* test. *, $P < 0.001$; **, $P = 0.006$; ***, $P = 0.003$. **D,** Cleaved caspase-3 immunoblotting showed increased apoptosis in IMR-32 cells when treated concomitantly with temozolomide and olaparib. **E,** IMR-32 cells were grown for 1 day in the presence or absence of temozolomide (100 µmol/L) and olaparib (1 µmol/L) and in the presence or absence of the pan-caspase inhibitor Z-VAD-FMK (20 µmol/L), as indicated. Growth and survival assays with XTT were determined. Statistical significance was determined by *t* test. *, $P < 0.001$.

development of the disease. Sequencing results on other genes included in the study and involved in DNA repair such as *BRCA1*, *BRCA2*, and Fanconi anemia complex genes such as *BRIP1*, *FANCA*, *FANCD2*, and *FANCE*, did not show any rare variants in any of the 17 neuroblastomas analyzed. However, other DNA repair genes such as *PRKDC* (*DNA-PK*), *BARD1*, *RAD51*, *FAM175A* (*ABRAXAS1*), and others were not included in the study and thus we cannot exclude that they may influence somehow the moderation of *ATM* allelic rare variants.

Alternatively, haploinsufficiency of genes located in 11q region may explain how loss of this region impacts disease outcome. Early studies on *ATM* haploinsufficiency revealed that heterozygosity for *ATM* predisposes to cataracts when the eye is exposed to ionizing radiation (41). *ATM* haploinsufficiency coincides with lower ATM expression in mouse fibroblasts and confers sensitivity to radiation when combined with *RAD9A* haploinssufficiency (42), a gene located in human chromosome 11q13. However, deletions of 11q region did not overlap *RAD9A locus* in our cohort of neuroblastoma patients (Supplementary Fig. S1). Notably, haploinsufficiency of *ATM* in neuroblastoma correlates with lower ATM expression, event-free survival, and overall survival (14). Consistent with this, our results demonstrate that cell lines that express low levels of ATM display increased sensitivity to the DNA-damaging drug temozolomide combined with PARP inhibition. Following this line of reasoning, one interesting possibility is that haploinsufficiency for *ATM* may be enhanced when combined with *H2AFX* and/or *MRE11A*. We observed that *ATM*, *H2AFX* and *MRE11A* are frequently included within the deleted

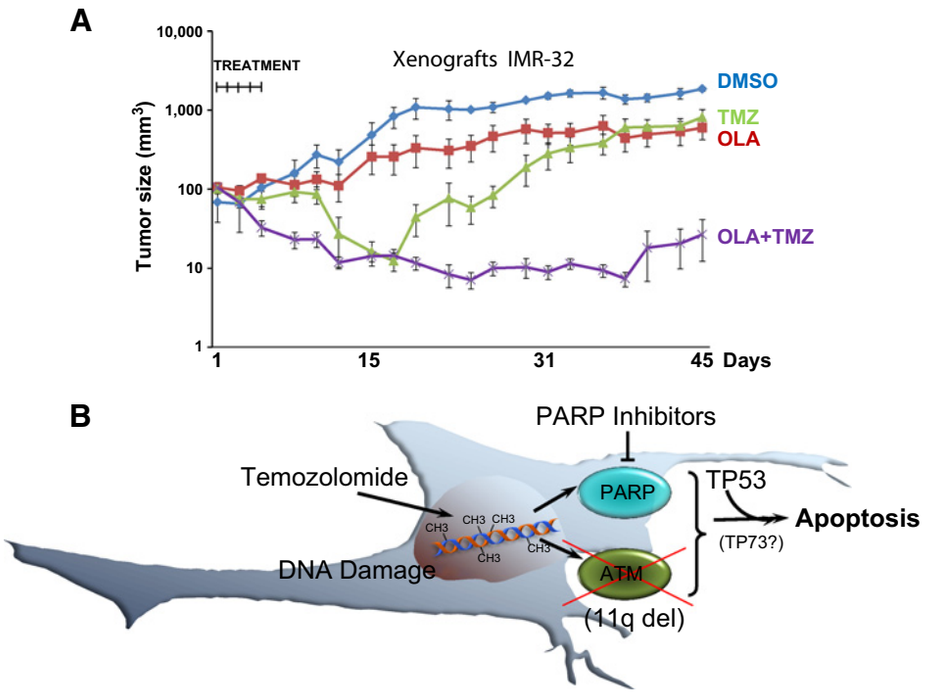

Figure 5.
Concomitant treatment of olaparib and temozolomide potently inhibits xenograft growth in nu/nu mice. **A,** Xenografts were generated by subcutaneous injection of 1.5×10^7 IMR-32 cells in 0.2 mL PBS:Matrigel (1:1). Two weeks later, mice were orally treated with olaparib (10 mg/kg) and/or temozolomide (50 mg/kg; control vehicle alone) for five consecutive days. Linear regression model with splines was performed to assess the interaction between day and treatment variables: $P < 0.001$ for DMSO versus olaparib (OLA); $P < 0.001$ for DMSO versus TMZ; $P < 0.001$ for DMSO versus olaparib + temozolomide. **B,** Predictive model for the genetic requirements of a neuroblastoma cell displaying sensitivity to olaparib and temozolomide. In the presence of DNA alkylating agent temozolomide and PARP inhibitor olaparib, cells lacking functional ATM are promoted to a TP53-dependent apoptosis.

region in 11q. Therefore, combined haploinsufficiency may result in poor expression levels in these three molecular regulators of DNA double-strand breaks repairing pathway and thus, compromise the whole repairing process.

ATM belongs to a family of genes implicated in DNA repair and maintenance of genomic integrity. In addition to *ATM*, *BRCA1* and *BRCA2* are also implicated in the repair of double-strand DNA breaks through homologous recombination (43). *PARP* plays an important role in DNA repair, but in contrast to *ATM* and *BRCAs*, *PARP* is activated by a mechanism regulating single-strand breaks. Pharmacologic inhibition of PARP induces cellular death in cancer cells with inactivating mutations in *BRCA* genes and is currently been used in therapy of breast and ovarian cancers with *BRCA* mutations (44). On the basis of the functional similarities between BRCAs and ATM, we hypothesized that neuroblastomas with 11q deletion would be highly susceptible to conventional chemotherapy when concomitantly treated with PARP inhibitors. Genomic studies of 11q-loss tumors revealed that loss of 4p and gain of 7q occurred at a significantly higher frequency in this subtype, but miRNA expression profile differentiated two 11q-loss subgroups with significantly different clinical outcome, with the poor survival subgroup having significantly more imbalances (5). Thus, it is possible that mutated *ATM* is associated with the group that displays more genetic instability. However, in our study, the imbalances in 4p or 7q were equally distributed: 5 patients among those with identified variant in *ATM* and 6 patients in the group in which we did not find any *ATM* variants. A published study of expression profile in 11q-loss neuroblastomas identified two biological subgroups that differ both in their clinical phenotype and gene expression patterns (4). On the basis of our current data, the presence of *ATM* variants with different activities and/or expression levels may reflect the differences observed in these two biological groups. Our tumor analysis revealed that about 50% of the patients contain a variant in *ATM*. The *in vitro* data from our study of cell lines with 11q deletion and the pharmacologic studies with the ATM kinase inhibitor strongly support a role for *ATM* haploinsufficiency in mediating sensitivity to temozolomide and olaparib. All 11q-deleted patients displayed additional segmental chromosomal breaks (Supplementary Fig. S1). However, only 2 of 17 showed chromothripsis (Supplementary Fig. S2), indicating that genes located within 11q deletion are not directly involved in the molecular mechanisms of chromothripsis and therefore, DNA repair and chromothripsis do not share strictly the same biological processes.

Olaparib treatment in neuroblastomas has recently been explored by enhancing its biological activity with either nitrofuran or with radiotherapy (45, 46). Olaparib has also been studied in combination with camptothecin, irinotecan, and its active metabolite SN38 (47), showing higher resistance in SK-N-AS cells. However, none of these reports included a parallel analysis of genetics which is essential to understanding the molecular basis of resistance to treatment. In addition to 11q deletion, IMR-32 and NBL-S cells display *MYCN* amplification (Supplementary Fig. S3) and both were sensible to the treatment. Although 11q deletion rarely occurs concomitantly with *MYCN* amplification (we identified only 6 neuroblastomas out of 418 patients with both alterations), our results demonstrate that sensitivity to olaparib + temozolomide therapy is governed by 11q deletion and hence, these rare patients would also benefit from the treatment. Collectively, the current findings emphasize tumor genotyping as key to precision medicine and strongly support the combined use of olaparib + temozolomide regimen for neuroblastomas with display both 11q deletion and functional TP53 (Fig. 5B).

Here we report that ectopic expression of wild-type *TP53* restored sensitivity to temozolomide and olaparib in the 11q-loss cell line SK-N-AS. Conversely, knock down of TP53 expression or activity in IMR-32 cells and in NBL-S cells resulted in decreased cleaved caspase-3. Moreover, temozolomide and olaparib treatment increased TP53 expression levels. Taken together, these results suggest that the principal mechanism of action of the combined treatment is induction of apoptosis through TP53 (Fig. 5B). *TP73* is a *TP53*-related tumor suppressor that is abundantly expressed in developing neurons and overexpression of its isoform ΔNp73 in neuroblastoma cells promotes cell survival by competing with other transcriptionally active isoform TAp73 as well as with TP53 (48). Therefore, although *TP73* mutations are infrequent in tumors, the frequent deletion of chromosome 1p in neuroblastomas where *TP73* is localized may also reflect a negative feedback mechanism for *TP53*. Collectively, our results suggest that patients with 11q-loss neuroblastomas may benefit from temozolomide and olaparib treatment and therefore, identification of patients likely to respond to this therapy will require a genetic analysis of tumors as part of a precision medicine strategy.

Disclosure of Potential Conflicts of Interest

No potential conflicts of interest were disclosed.

Authors' Contributions

Conception and design: A. Cañete, V. Castel, J. Font de Mora
Development of methodology: E. Sanmartín, L. Muñoz, M. Piqueras, J.A. Sirerol, P. Berlanga, J. Font de Mora
Acquisition of data (provided animals, acquired and managed patients, provided facilities, etc.): L. Muñoz, J.A. Sirerol, V. Castel, J. Font de Mora
Analysis and interpretation of data (e.g., statistical analysis, biostatistics, computational analysis): E. Sanmartín, L. Muñoz, M. Piqueras, J.A. Sirerol, P. Berlanga, V. Castel, J. Font de Mora
Writing, review, and/or revision of the manuscript: E. Sanmartín, P. Berlanga, A. Cañete, V. Castel, J. Font de Mora
Administrative, technical, or material support (i.e., reporting or organizing data, constructing databases): E. Sanmartín, M. Piqueras, J.A. Sirerol, V. Castel, J. Font de Mora
Study supervision: E. Sanmartín, L. Muñoz, J. Font de Mora

Acknowledgments

We thank D. Ramal (Pediatric Oncology Clinical Trials Unit, University Hospital La Fe) for update and support on patients' data analyzed in Fig. 1 and Table 1, and the staff members at Genomics Unit for support in the analysis of sequencing data. We are grateful to S. Zuñiga and A. Marco for informatics support in generation of circos plots and to V. Fornés-Ferrer for assistance with statistics. We are also thankful to AstraZeneca for providing olaparib for these studies.

Grant Support

Research conducted in the authors' laboratories was supported by Asociación Pablo Ugarte (APU) and by grant from Conselleria d'Educació GVA Prometeo 2012/060 and grant from Fundación Científica de la Asociación Española Contra el Cáncer (AECC 2016).

The costs of publication of this article were defrayed in part by the payment of page charges. This article must therefore be hereby marked *advertisement* in accordance with 18 U.S.C. Section 1734 solely to indicate this fact.

Received February 28, 2017; revised June 23, 2017; accepted August 16, 2017; published OnlineFirst August 22, 2017.

References

1. Spitz R, Hero B, Ernestus K, Berthold F. FISH analyses for alterations in chromosomes 1, 2, 3, and 11 define high-risk groups in neuroblastoma. Med Pediatr Oncol 2003;41:30–5.
2. McArdle L, McDermott M, Purcell R, Grehan D, O'Meara A, Breatnach F, et al. Oligonucleotide microarray analysis of gene expression in neuroblastoma displaying loss of chromosome 11q. Carcinogenesis 2004;25:1599–609.
3. Spitz R, Hero B, Simon T, Berthold F. Loss in chromosome 11q identifies tumors with increased risk for metastatic relapses in localized and 4S neuroblastoma. Clin Cancer Res 2006;12:3368–73.
4. Fischer M, Bauer T, Oberthur A, Hero B, Theissen J, Ehrich M, et al. Integrated genomic profiling identifies two distinct molecular subtypes with divergent outcome in neuroblastoma with loss of chromosome 11q. Oncogene 2010;29:865–75.
5. Buckley PG, Alcock L, Bryan K, Bray I, Schulte JH, Schramm A, et al. Chromosomal and microRNA expression patterns reveal biologically distinct subgroups of 11q- neuroblastoma. Clin Cancer Res 2010;16:2971–8.
6. Santo EE, Ebus ME, Koster J, Schulte JH, Lakeman A, van Sluis P, et al. Oncogenic activation of FOXR1 by 11q23 intrachromosomal deletion-fusions in neuroblastoma. Oncogene 2012;31:1571–81.
7. Wang Q, Diskin S, Rappaport E, Attiyeh E, Mosse Y, Shue D, et al. Integrative genomics identifies distinct molecular classes of neuroblastoma and shows that multiple genes are targeted by regional alterations in DNA copy number. Cancer Res 2006;66:6050–62.
8. Caren H, Kryh H, Nethander M, Sjoberg RM, Trager C, Nilsson S, et al. High-risk neuroblastoma tumors with 11q-deletion display a poor prognostic, chromosome instability phenotype with later onset. Proc Natl Acad Sci U S A 2010;107:4323–8.
9. Ando K, Ohira M, Ozaki T, Nakagawa A, Akazawa K, Suenaga Y, et al. Expression of TSLC1, a candidate tumor suppressor gene mapped to chromosome 11q23, is downregulated in unfavorable neuroblastoma without promoter hypermethylation. Int J Cancer 2008;123:2087–94.
10. Caren H, Holmstrand A, Sjoberg RM, Martinsson T. The two human homologues of yeast UFD2 ubiquitination factor, UBE4A and UBE4B, are located in common neuroblastoma deletion regions and are subject to mutations in tumours. Eur J Cancer 2006;42:381–7.
11. Hammerle B, Yanez Y, Palanca S, Canete A, Burks DJ, Castel V, et al. Targeting neuroblastoma stem cells with retinoic acid and proteasome inhibitor. PLoS One 2013;8:e76761.
12. Canete A, Gerrard M, Rubie H, Castel V, Di Cataldo A, Munzer C, et al. Poor survival for infants with MYCN-amplified metastatic neuroblastoma despite intensified treatment: the international society of paediatric oncology european neuroblastoma experience. J Clin Oncol 2009;27:1014–9.
13. Guo C, White PS, Weiss MJ, Hogarty MD, Thompson PM, Stram DO, et al. Allelic deletion at 11q23 is common in MYCN single copy neuroblastomas. Oncogene 1999;18:4948–57.
14. Mandriota SJ, Valentijn LJ, Lesne L, Betts DR, Marino D, Boudal-Khoshbeen M, et al. Ataxia-telangiectasia mutated (ATM) silencing promotes neuroblastoma progression through a MYCN independent mechanism. Oncotarget 2015;6:18558–76.
15. Cohn SL, Pearson AD, London WB, Monclair T, Ambros PF, Brodeur GM, et al. The international neuroblastoma risk group (INRG) classification system: an INRG Task Force report. J Clin Oncol 2009;27:289–97.
16. Burgues O, Navarro S, Noguera R, Pellin A, Ruiz A, Castel V, et al. Prognostic value of the international neuroblastoma pathology classification in neuroblastoma (Schwannian stroma-poor) and comparison with other prognostic factors: a study of 182 cases from the Spanish Neuroblastoma Registry. Virchows Archiv 2006;449:410–20.
17. Shimada H, Ambros IM, Dehner LP, Hata J, Joshi VV, Roald B, et al. The International neuroblastoma pathology classification (the Shimada system). Cancer 1999;86:364–72.
18. Ambros IM, Benard J, Boavida M, Bown N, Caron H, Combaret V, et al. Quality assessment of genetic markers used for therapy stratification. J Clin Oncol 2003;21:2077–84.

19. Noguera R, Canete A, Pellin A, Ruiz A, Tasso M, Navarro S, et al. MYCN gain and MYCN amplification in a stage 4S neuroblastoma. Cancer Genet Cytogenet 2003;140:157–61.
20. Ambros IM, Brunner C, Abbasi R, Frech C, Ambros PF. Ultra-High density SNParray in neuroblastoma molecular diagnostics. Front Oncol 2014; 4:202.
21. Robinson JT, Thorvaldsdottir H, Winckler W, Guttman M, Lander ES, Getz G, et al. Integrative genomics viewer. Nat Biotechnol 2011;29:24–6.
22. Li H, Durbin R. Fast and accurate short read alignment with Burrows-Wheeler transform. Bioinformatics 2009;25:1754–60.
23. DePristo MA, Banks E, Poplin R, Garimella KV, Maguire JR, Hartl C, et al. A framework for variation discovery and genotyping using next-generation DNA sequencing data. Nat Genet 2011;43:491–8.
24. Xu SP, Sun GP, Shen YX, Peng WR, Wang H, Wei W. Synergistic effect of combining paeonol and cisplatin on apoptotic induction of human hepatoma cell lines. Acta Pharmacologica Sinica 2007;28:869–78.
25. Tomayko MM, Reynolds CP. Determination of subcutaneous tumor size in athymic (nude) mice. Cancer Chemother Pharmacol 1989;24:148–54.
26. Guo C, White PS, Hogarty MD, Brodeur GM, Gerbing R, Stram DO, et al. Deletion of 11q23 is a frequent event in the evolution of MYCN single-copy high-risk neuroblastomas. Med Pediatr Oncol 2000;35:544–6.
27. Vandesompele J, Speleman F, Van Roy N, Laureys G, Brinskchmidt C, Christiansen H, et al. Multicentre analysis of patterns of DNA gains and losses in 204 neuroblastoma tumors: how many genetic subgroups are there? Med Pediatr Oncol 2001;36:5–10.
28. Weston VJ, Oldreive CE, Skowronska A, Oscier DG, Pratt G, Dyer MJ, et al. The PARP inhibitor olaparib induces significant killing of ATM-deficient lymphoid tumor cells *in vitro* and *in vivo*. Blood 2010;116:4578–87.
29. Williamson CT, Kubota E, Hamill JD, Klimowicz A, Ye R, Muzik H, et al. Enhanced cytotoxicity of PARP inhibition in mantle cell lymphoma harbouring mutations in both ATM and p53. EMBO Mol Med 2012;4:515–27.
30. Mazot P, Cazes A, Dingli F, Degoutin J, Irinopoulou T, Boutterin MC, et al. Internalization and down-regulation of the ALK receptor in neuroblastoma cell lines upon monoclonal antibodies treatment. PLoS One 2012;7: e33581.
31. Goldschneider D, Horvilleur E, Plassa LF, Guillaud-Bataille M, Million K, Wittmer-Dupret E, et al. Expression of C-terminal deleted p53 isoforms in neuroblastoma. Nucleic Acids Res 2006;34:5603–12.
32. Van Maerken T, Rihani A, Dreidax D, De Clercq S, Yigit N, Marine JC, et al. Functional analysis of the p53 pathway in neuroblastoma cells using the small-molecule MDM2 antagonist nutlin-3. Mol Cancer Ther 2011;10: 983–93.
33. Thiele CJ.Neuroblastoma cell lines. In: Masters J, editor. Human cell culture. Lancaster, United Kingdom: Kluwer Academic Publishers; 1998. p. 21–53.
34. Spieker N, van Sluis P, Beitsma M, Boon K, van Schaik BD, van Kampen AH, et al. The MEIS1 oncogene is highly expressed in neuroblastoma and amplified in cell line IMR32. Genomics 2001;71:214–21.
35. Stewart E, Goshorn R, Bradley C, Griffiths LM, Benavente C, Twarog NR, et al. Targeting the DNA repair pathway in Ewing sarcoma. Cell Rep 2014; 9:829–41.
36. Liberzon E, Avigad S, Yaniv I, Stark B, Avrahami G, Goshen Y, et al. Molecular variants of the ATM gene in Hodgkin's disease in children. Br J Cancer 2004;90:522–5.
37. Liberzon E, Avigad S, Stark B, Zilberstein J, Freedman L, Gorfine M, et al. Germ-line ATM gene alterations are associated with susceptibility to sporadic T-cell acute lymphoblastic leukemia in children. Genes Chromosomes Cancer 2004;39:161–6.
38. Rudd MF, Sellick GS, Webb EL, Catovsky D, Houlston RS. Variants in the ATM-BRCA2-CHEK2 axis predispose to chronic lymphocytic leukemia. Blood 2006;108:638–44.
39. Sanmartin E, Yanez Y, Fornes-Ferrer V, Zugaza JL, Canete A, Castel V, et al. TIAM1 variants improve clinical outcome in neuroblastoma. Oncotarget 2017;8:45286–97.
40. Schaffner C, Stilgenbauer S, Rappold GA, Dohner H, Lichter P. Somatic ATM mutations indicate a pathogenic role of ATM in B-cell chronic lymphocytic leukemia. Blood 1999;94:748–53.
41. Barlow C, Eckhaus MA, Schaffer AA, Wynshaw-Boris A. Atm haploinsufficiency results in increased sensitivity to sublethal doses of ionizing radiation in mice. Nat Genet 1999;21:359–60.
42. Smilenov LB, Lieberman HB, Mitchell SA, Baker RA, Hopkins KM, Hall EJ. Combined haploinsufficiency for ATM and RAD9 as a factor in cell transformation, apoptosis, and DNA lesion repair dynamics. Cancer Res 2005;65:933–8.
43. Murphy CG, Moynahan ME. BRCA gene structure and function in tumor suppression: a repair-centric perspective. Cancer J 2010;16:39–47.
44. Helleday T.The underlying mechanism for the PARP and BRCA synthetic lethality: clearing up the misunderstandings. Mol Oncol 2011;5:387–93.
45. McNeil EM, Ritchie AM, Melton DW. The toxicity of nitrofuran compounds on melanoma and neuroblastoma cells is enhanced by Olaparib and ameliorated by melanin pigment. DNA Repair 2013;12:1000–6.
46. Nile DL, Rae C, Hyndman IJ, Gaze MN, Mairs RJ. An evaluation in vitro of PARP-1 inhibitors, rucaparib and olaparib, as radiosensitisers for the treatment of neuroblastoma. BMC Cancer 2016;16:621.
47. Norris RE, Adamson PC, Nguyen VT, Fox E. Preclinical evaluation of the PARP inhibitor, olaparib, in combination with cytotoxic chemotherapy in pediatric solid tumors. Pediatr Blood Cancer 2014;61:145–50.
48. Nakagawa T, Takahashi M, Ozaki T, Watanabe K, Hayashi S, Hosoda M, et al. Negative autoregulation of p73 and p53 by DeltaNp73 in regulating differentiation and survival of human neuroblastoma cells. Cancer Lett 2003;197:105–9.